Effect of spatio-temporal coupling on ultrafast laser direct writing in glass

Qin Li (李 沁)[1], Wenbo Li (李文博)[2], Wei Chu (储 蔚)[2], Yuxiang Cao (曹宇祥)[1], Wencheng Zhang (张文成)[1], Hongliang Ma (马洪良)[1], Zuanming Jin (金钻明)[1], and Ye Dai (戴 晔)[1,*]

[1]*Department of Physics, Shanghai University, Shanghai 200444, China*
[2]*State Key Laboratory of High Field Laser Physics, Shanghai Institute of Optics and Fine Mechanics, Chinese Academy of Sciences, Shanghai 201800, China*
**Corresponding author: yedai@shu.edu.cn*

Received January 23, 2019; accepted April 25, 2019; posted online July 4, 2019

Spatio-temporal coupling characteristics of ultrafast laser pulses are quantitatively tailored. An asymmetric microstructure is induced in the focal volume when the laser scans perpendicularly to the direction of the spatial chirp in fused silica. The tilted direction reverses when adding a Dove prism into the light path. The sign of the pulse front tilt can be turned from positive to negative by changing the group delay dispersion by steps. We reveal that the tilted direction of a microstructure depends on spatial chirp, and the interplay between spatio-temporal chirp leads to the change of tilted angles.

OCIS codes: 140.3390, 220.4000, 320.5540.
doi: 10.3788/COL201917.081402.

A femtosecond laser can be focused into transparent dielectrics to achieve the inscription process in three-dimensional (3D) space due to nonlinear multi-photon absorption induced by extremely high peak intensity[1–3]. The spatial resolution of micromachining is further improved for multi-photon absorption by just taking place in the center of the beam. So far, femtosecond laser micromachining has demonstrated a broad range of applications, such as optical waveguide[4–6], micro-optical elements[7], microchannels[8], and high-density data storage[9]. Recent research, however, shows that nonlinear propagation on the way to the target zone is possible to hamper efficient ablation or the modification of transparent materials near the focus[10,11]. In order to address the issue, tailoring spatio-temporally focused ultrafast laser pulses attracts great attention now. Initially, the technology was aimed at improving the signal-to-background ratio in multi-photon microscopy[12,13]. Its core idea is that spectral components of incident pulse can be spatially separated after an optical stretcher and then recombine only at the spatial focus after an objective. By this means, pulse width becomes a function of distance, with the shortest pulse width confined to the spatial focus. Once out of focus, the pulse width will increase rapidly so that the intensity is insufficient to reach critical power for material modification[14]. The spatio-temporal coupling of ultrafast laser pulses provides an effective approach to efficiently suppress the optical aberration and achieve a nearly invariant spatial resolution for a large range of penetration depths between 250 μm and 9 mm in glass[15]. When focusing into the sample at a larger depth, temporal focusing with spatio-temporal coupling is much more robust than the conventional focusing (CF) method in temporal pulse width and peak intensity in the focal volume[16].

In general, effects of spatio-temporal coupling on ultrafast laser direct writing could result from a combination of spatial chirp (SC) and temporal chirp (TC) or angular dispersion (AD), which leads to a tilt of the pulse intensity front known as the pulse front tilt (PFT)[17]. The optimal positively chirped pump laser pulses optimized the highly efficient terahertz generation[18]. Previously, the PFT has been generally considered to dominate an intriguing quill effect, which was firstly proposed by Kazansky *et al.*[19]. Simply reversing the scanning direction can lead to an obvious difference in the birefringence intensity and the transverse length of the written structures. Vitek *et al.* also utilized a simultaneous spatial and temporal focusing (SSTF) system to achieve the PFT value up to 16,000 fs/mm for nonreciprocal writing in glass[20]. Our group researched influences of the quill effect on the self-organized nanograting formation and then found 3D rotation of nanograting inside fused silica[21,22]. Recently the transient plasma track induced by the SSTF pulses shows it to be significantly curved in the focal volume using a pump–probe shadow imaging technique, and the phenomenon is attributed to an asymmetric carrier density distribution along the PFT plane[23]. Guan *et al.* reported the quill effect in the waveguide writing regime with the help of adaptive third harmonic generation microscopy[24]. However, as the research progresses, the quill effect is also regarded as a result of AD at the focus rather than the correlated PFT[25]. Therefore, the effects of spatio-temporal coupling on ultrafast laser direct writing have not been fully elucidated. The mechanism behind the quill phenomena needs further study.

In this Letter, we make use of a femtosecond laser SSTF system to study how the PFT affects the written microstructures in fused silica. Spatio-temporal characteristics

of the focusing laser pulses could be quantitatively adjusted by adding a Dove prism or adjusting internal and external pulse compressors. We could also reverse the sign of PFT before the objective by altering the optical distance between a pair of gratings. When laser scanning direction was perpendicular to the SC direction of the laser, asymmetric microstructures with tilted heads were formed by observing transverse sections of the written lines. Furthermore, the tilted direction could flip over 180° when the SC direction was fully reversed. Besides, the tilted angle shows a difference but keeps toward the same side when the increased group delay dispersion (GDD) causes a change of the PFT. Present research paves a new way to fabricate integrated optical elements by manipulating the light field of an ultrafast laser.

Figure 1 shows a schematic of the experimental setup. A 1 kHz repetition rate Ti:sapphire regenerative laser amplifier system (Spitfire, Spectra-physics Co.) delivers a 120 fs laser pulse at a center wavelength of 800 nm with a spectral bandwidth of 10 nm. The laser was linearly polarized along the Y direction. An adjustable circular aperture was employed to control the input laser beam size of about 2.6 mm. A variable neutral density filter was set in the light path to adjust the pulse energy. The incident angle of the first grating (G1) was 25°; a pair of gratings (600 line/mm) could separate the spectral components of the incident beam along the Y axis and collimate the beam with the SC and TC. To verify a spatial broadening of a shaped pulse, 2 two-dimensional (2D) intensity distributions of a laser beam profile (SP503U, Ophir-Spiricon), respectively, were measured in front of and behind the grating pair. The distance between gratings can vary from 37.5 to 117.5 mm to tailor the spatio-temporal characteristics of the pulses. Unless otherwise specified, the gratings refer to the external ones. In the light path, the direction of the SC can be flipped over 180° by adding a Dove prism, which is usually used to rotate, invert, or retroreflect an image. Lastly, the shaped laser pulses were directed into an optical microscope system (Nikon ECLIPSE 80i) and then were focused into a fused silica sample by a 50 times objective (NA = 0.55). The computer-controlled 3D motorized stage (Prior Scientific, Optics Scan II) can move the sample at the focal depth of ~75 μm below the surface

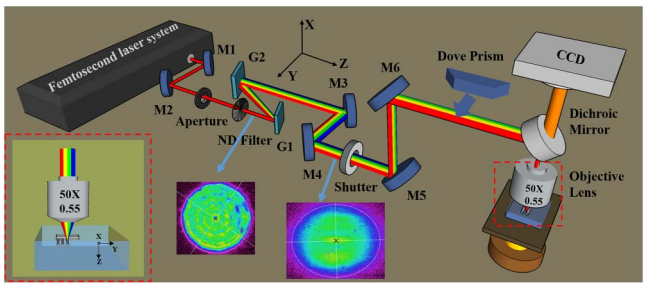

Fig. 1. Schematic diagram of the experimental setup. The insert demonstrates two scanning directions along X and Y, and the transmission direction is along Z. A red box surrounded by the dotted line represents processing sample details.

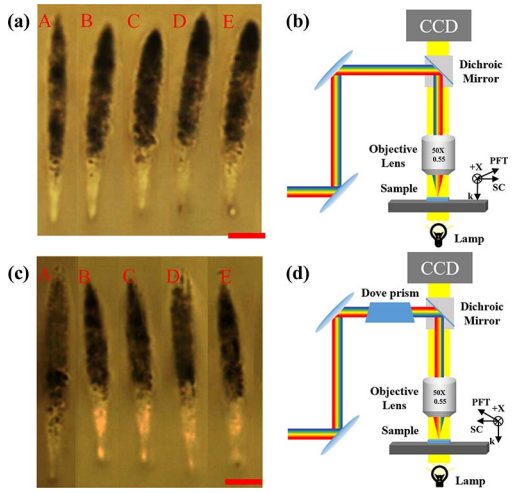

Fig. 2. (a) Optical images of transverse sections of the asymmetric microstructures with tilted heads induced by the laser pulses transmitting (b) without a Dove prism and (d) with a Dove prism. The type A microstructures in (a) and (c) are induced by a CF system. The type B to E ones are four groups of tilted microstructures induced by the SSTF pulses with varying grating distances. The red bar is 5 μm.

of the sample and scan lines with set parameters. Two groups of written lines were inscribed at a scanning speed of 5 μm/s along the X axis and Y axis, respectively. We also set up a CF system to directly write the lines as a contrast experiment.

Figure 2 demonstrates the transverse sections of two series of written lines without and with a Dove prism in the light path after laser scanning perpendicular to the direction of the SC. The pulse energy after the objective is 0.6 μJ. The type A microstructures in Figs. 2(a) and 2(c) show common structures induced by the CF system without and with a Dove prism. The modified shape is perfectly straight and symmetric. Figures 2(b) and 2(d) are schematic diagrams of the SSTF system for the induced type B to E microstructures in Figs. 2(a) and 2(c). In this situation, the SC is parallel to the frequency gradient of the spatially broadening pulse, and the direction is from the high-frequency component to the low-frequency component of light. Also, the direction of the PFT is in accordance with that of the SC. Once the SC direction is chosen, the sign of the PFT only depends on the sign of the GDD of the shaped pulses. The PFT value can be roughly represented by the angle between the PFT and SC. Figure 2(a) types B–E show four transverse sections of written lines by the SSTF pulses with increasing grating distances of 52.5, 57.5, 62.5, and 67.5 mm, respectively. It is noted that obvious tilt occurs on the head of each structure modification, but their tilted directions remain unchanged even if the grating distances are different. As a contrast, Fig. 2(c) types B–E show the other tilted microstructures whose directions are apparently opposite that of Fig. 2(a) types B–E. The phenomenon is very intriguing because we only added a Dove prism in the light path, which makes the SC direction flip over 180° before the

objective by reversing the frequency gradient of pulses. Since the flip of the SC can further lead to the flip of the PFT, while the sign of PFT is determined by both SC and TC, it is still uncertain how the TC affects the tilt of the microstructures. Therefore, we kept the SC direction unchanged, but changed the GDD of the shaped pulses to change the sign of the PFT.

The GDDs of shaped pulses could be pre-compensated by adjusting a grating compressor in a double pass geometry, which was incorporated into the laser cavity. Then, the pre-chirped femtosecond laser pulses could further change their GDDs by varying the distance between a pair of external gratings from 37.5 to 82.5 mm with 5 mm intervals per step. The temporal duration was measured behind the second grating, as shown in Fig. 3. The pulse duration was set to 222 fs initially when the pulses exported from the laser amplifier system. With the grating distance increasing, the pulse duration gradually shortened at first and then turned to be longer. The shortest pulse duration was 130 fs, which was close to the ideal pulse duration of the laser system emissions. As a pair of parallel gratings always introduces negative GDD, it is reasonable that the sign of the initial chirp of femtosecond laser pulses is positive. The value of GDD introduced by gratings is given by[26]

$$\mathrm{GDD} = \frac{\mathrm{d}^2\phi_c(\omega)}{\mathrm{d}\omega^2} = \frac{\lambda^3 L_g}{2\pi c^2 \mathrm{d}^2}\left[1 - \left(\frac{\lambda}{d} - \sin\gamma\right)^2\right]^{-3/2}. \quad (1)$$

According to calculations with the incident parameters in this case, we get a compact expression for the changed $\mathrm{GDD} = -352.896 L_g$, where L_g is the distance between a pair of gratings. After summing both the pre-compensated and adjustable GDD, the sign of GDD can change from positive to negative at the objective entrance.

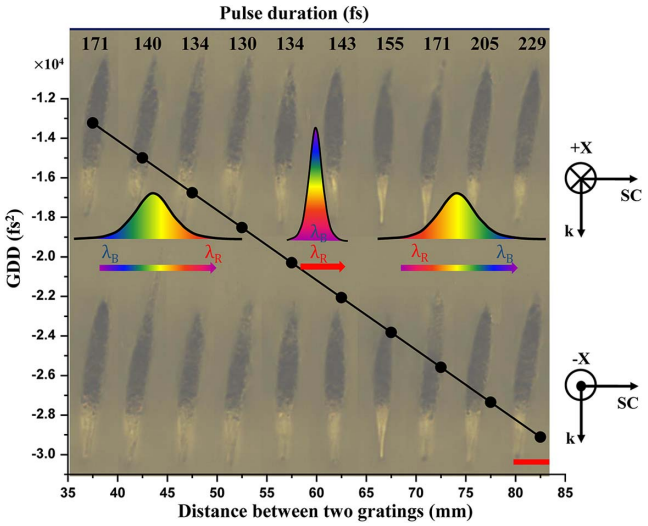

Fig. 3. Optical images of transverse sections of written lines with different tilted angles. Two scanning directions are, respectively, along $+X$ and $-X$. Dependence of the introduced GDD on the grating distances is shown by the black solid line. The top coordinate presents a trend of pulse duration, which was measured behind the gratings. The pulse profiles show three states of TC by changing the GDD. The red bar is 5 μm.

Generally, the PFT can be presented as the following[27]:

$$P = P_{\mathrm{AD}} + P_{\mathrm{SC+TC}}. \quad (2)$$

PFT consists of a term of AD and a mixed term of SC and TC. When the shaped pulse is behind a pair of gratings but before the objective, the PFT is mainly caused by the second term $P_{\mathrm{SC+TC}}$, while the AD is negligible. As shown in Fig. 3, the tilted angle of the head on each induced microstructure is gradually smaller with an increase of distance at the beginning and then turns out to be larger when the distance is longer than 62.5 mm. But, the tilted direction always keeps toward the same side. Since the positive dispersion medium (e.g., the objective) behind the gratings would continue to introduce a positive GDD in addition to the pre-compensated positive one, when the grating distance is 62.5 mm, the GDD behind the objective is considered to be 0 fs^2 due to the offset of negative GDD resulting from the gratings. Therefore, a straight structure is induced. Another grating distance of 52.5 mm is also worth noting, because the pulse duration is the shortest at 130 fs, but the induced structure remains tilted. This further implies that an extra positive GDD can be introduced when the pulse goes through the objective. The variation of GDD is between 8800 and −7000 when the grating distance changes from 37.5 to 82.5 mm, which can lead to a change of the sign of the PFT from positive to negative. Considering that the tilted direction is unchanged in spite of varying GDD and PFT, it can verify that the SC of the shaped pulse is the key parameter to determine the tilt direction of the asymmetric microstructure.

We further consider the evolution of PFT in the focusing process with different PFTs in the beginning. Figure 4(a) shows the evolution of PFT near the focus along the light transmission direction. Different PFTs are defined by a combination of the same SC and various GDDs, including -4000 fs^2 (blue line), -3000 fs^2 (purple line), 0 fs^2 (black line), 3000 fs^2 (green line), and 4000 fs^2 (red line). As it has been proven, PFT will always be -16.8 fs/μm at the focus as a result of different spectral components overlapping[17,28]. So, the PFT value at the focus strongly depends on the inherent SC at the objective entrance, independent of the focusing conditions[28]. The main reason is that focusing introduces a finite AD and makes the spectral components overlap near the focus; the PFT originating from the AD becomes gradually prominent, even in the case of zero PFT. As for the changing trend of the tilted angle, we need to estimate where the PFT affects the tilted angle. Figure 4(b) shows the relative intensity evolution of different PFT cases near the focus. Obviously, the maximum focal intensity in the zero PFT case is above twice that in the non-zero PFT cases. Comparing the relative intensities between the zero PFT case and non-zero PFT cases, the PFT = 0 case can reach a damage threshold before the non-zero PFT cases.

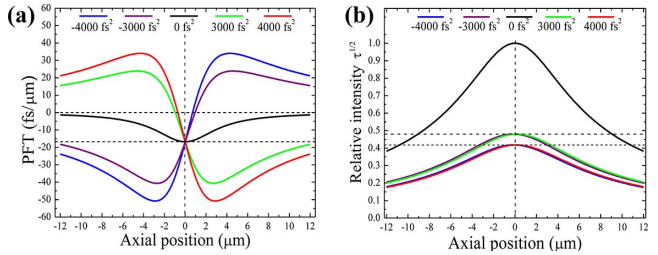

Fig. 4. (a) Evolution of PFT along focusing for five different GDD cases. The SC will disappear because the laser beam converges to a point. The PFT with different GDD is all about −16.8 fs/μm at the focal plane when PFT depends on the AD. (b) Relative intensity threshold evolution during focusing for the five cases. The zero GDD case (black line) is larger than other cases and symmetric on the focus. When the GDD is positive, the peak intensity slightly moves to the left side of the axis with $X = 0$. The situation is opposite when the GDD is negative. Regardless of the positive or negative non-zero GDD cases, the peak intensity of different GDD cases with the same value is identical. The peak intensity is lower with the GDD increasing.

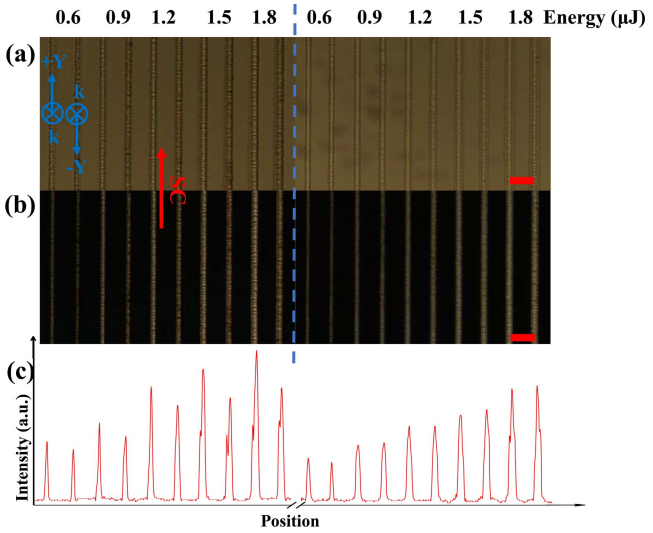

Fig. 5. Optical microscope images of the written lines with various pulse energies in the cases of CF (right) and SSTF (left) systems. Two lines of each group were independently written along $+Y$ and $-Y$. k indicates the directions of the laser propagation. (a) Ordinary optical images. (b) Birefringence of the lines under cross-polarization illumination. (c) The relative intensity variation of the birefringence signal from the written lines. The red bar is 20 μm.

It means that the structural modification from zero PFT can take place at a long distance relative to the focus. From Fig. 4(b), the changing trend of PFT in the GDD case with $-3000\,\mathrm{fs}^2$ also reveals that the structure modification could happen at the place before the focal plane, where the pulse has a maximum intensity and a negative PFT. Correspondingly, the modification happens behind the focal plane where the PFT turns negative in the GDD case with $+3000\ \mathrm{fs}^2$. Therefore, both of the negative PFTs will induce tilted structures toward the same side. During processing, the PFT can establish a tilted intensity plane, which pushes an excited plasma to spread along the front. In the presence of intensity gradients, the ponderomotive force expels the free electrons from the region of high intensity[19]. Then, an asymmetrical carrier motion and successive defect distribution could form in the modification area. The gradient of the refractive index in fused silica induced by plasma is closely related to the magnitude of plasma density[23], leading to localized plasma density on one side that is sufficient for bending the propagation trajectory of the femtosecond pulses and causes tilted modifications. So, the PFT value could make a difference on the tilted angle.

Figure 5 shows an obvious quill effect on the written lines parallel to the direction of SC: the laser along $+Y$ and $-Y$, respectively. The distance between a pair of gratings is fixed at 67.5 mm in order to cause the spatial broadening of pulses and then the PFT. The cross-polarized image in Fig. 5(b) presents a birefringence phenomenon because of the formation of the self-organized nanograting, and the intensity increases with an increase of the incident pulse energy. Figure 5(c) reveals the intensity variation of the birefringence signal of written lines along $+Y$ and $-Y$ by using an SSTF system. As a comparison, there is nearly no difference in relative intensity between two lines written by a CF system with opposite scanning directions. The experiment result verifies again that the PFT generated from the SC of the shaped pulse by an SSTF system can induce the nonreciprocal writing phenomenon in glass.

In summary, we used an SSTF system to introduce adjustable spatio-temporal coupling of femtosecond pulses to study the quill effect in fused silica. When the scanning direction is perpendicular to the SC direction of the shaped pulse, tilted microstructures are induced in the focal volume. Besides, adding a Dove prism in the light path results in the flip of the tilted direction due to the reverse of the SC direction. A quantitative analysis is further made on the dependence of tilted angles on the GDD of the shaped pulse, and we discover that the tilted direction stays unchanged even if the sign of PFT turns with the introduced GDD increasing, but the tilted angles show a difference as a result of a change of the PFT value. Our result provides a significant insight into the quill writing phenomenon and can deepen the understanding of the effect of spatio-temporal coupling on ultrafast laser direct writing.

This work was supported by the National Natural Science Foundation of China (NSFC) (Nos. 11774220, 11604202, and 61735010).

References

1. F. Zhang, A. Cerkauskaite, R. Drevinskas, P. G. Kazansky, and J. Qiu, Adv. Opt. Mater. **5**, 1700342 (2017).
2. Y. Tan, Z. Wang, W. Chu, Y. Liao, L. Qiao, and Y. Cheng, Opt. Mater. Express **6**, 3787 (2016).

3. Y. Dai, A. Patel, J. Song, M. Beresna, and P. G. Kazansky, Opt. Express **24**, 19344 (2016).
4. P. S. Salter, M. J. Woolley, S. M. Morris, M. J. Booth, and J. A. J. Fells, Opt. Lett. **43**, 5993 (2018).
5. J. Lu, Y. Dai, Q. Li, Y. Zhang, C. Wang, F. Pang, T. Wang, and X. Zeng, Nanoscale **11**, 908 (2019).
6. Y. Jia and F. Chen, Chin. Opt. Lett. **17**, 012302 (2019).
7. F. He, Y. Cheng, L. Qiao, C. Wang, Z. Xu, K. Sugioka, K. Midorikawa, and J. Wu, Appl. Phys. Lett. **96**, 041108 (2010).
8. X. Sun, D. Cui, Y. Hu, D. Chu, G. Chen, J. Yu, J. Zhou, and J. Duan, Chin. Opt. Lett. **16**, 101402 (2018).
9. J. Zhang, M. Gecevičius, M. Beresna, and P. G. Kazansky, Phys. Rev. Lett. **112**, 033901 (2014).
10. R. Kammel, R. Ackermann, J. Thomas, J. Götte, S. Skupin, A. Tünnermann, and S. Nolte, Light: Sci. Appl. **3**, e169 (2014).
11. T. E. Lanier and J. R. Gulley, J. Opt. Soc. Am. B **33**, 292 (2016).
12. D. Oron, E. Tal, and Y. Silberberg, Opt. Express **13**, 1468 (2005).
13. G. Zhu, J. van Howe, M. Durst, W. Zipfel, and C. Xu, Opt. Express **13**, 2153 (2005).
14. G. Pariente, V. Gallet, A. Borot, O. Gobert, and F. Quéré, Nat. Photon. **10**, 547 (2016).
15. P. Wang, W. Chu, W. Li, Y. Tan, J. Qi, Y. Liao, Z. Wang, and Y. Cheng, Opt. Lett. **43**, 3485 (2018).
16. B. Sun, P. S. Salter, and M. J. Booth, J. Opt. Soc. Am. B **32**, 1272 (2015).
17. A. Patel, Y. Svirko, C. Durfee, and P. G. Kazansky, Sci. Rep. **7**, 12928 (2017).
18. X. Wu, S. Chai, J. Ma, B. Zhang, C. Xia, Z. Fang, D. Kong, J. Wang, H. Liu, C. Zhu, X. Wang, C. Ruan, and Y. Li, Chin. Opt. Lett. **16**, 041901 (2018).
19. P. G. Kazansky, W. Yang, E. Bricchi, J. Bovatsek, A. Arai, Y. Shimotsuma, K. Miura, and K. Hirao, Appl. Phys. Lett. **90**, 151120 (2007).
20. D. N. Vitek, E. Block, Y. Bellouard, D. E. Adams, S. Backus, D. Kleinfeld, C. G. Durfee, and J. A. Squier, Opt. Express **18**, 24673 (2010).
21. Y. Dai, G. Wu, X. Lin, G. Ma, and J. Qiu, Opt. Express **20**, 18072 (2012).
22. Y. Dai, J. Ye, M. Gong, X. Ye, X. Yan, G. Ma, and J. Qiu, Opt. Express **22**, 28500 (2014).
23. Z. H. Wang, B. Zeng, G. H. Li, H. Q. Xie, W. Chu, F. He, Y. Liao, W. W. Liu, H. Gao, and Y. Cheng, Opt. Lett. **40**, 5726 (2015).
24. J. Guan, X. Liu, and M. J. Booth, Opt. Express **26**, 30716 (2018).
25. C. G. Durfee, M. Greco, E. Block, D. Vitek, and J. A. Squier, Opt. Express **20**, 14244 (2012).
26. S. Backus, C. G. Durfee III, M. M. Murnane, and H. C. Kapteryn, Rev. Sci. Instrum. **69**, 1207 (1998).
27. S. Akturk, X. Gu, E. Zeek, and R. Trebino, Opt. Express **12**, 4399 (2004).
28. S. Zhang, D. Asoubar, R. Kammel, S. Nolte, and F. Wyrowski, J. Opt. Soc. Am. A **31**, 2437 (2014).